Science and Technology for Energy Transition **77**, 4 (2022)

https://doi.org/10.2516/stet/2022003

Selected Papers from 7th International Symposium on Hydrogen Energy, Renewable Energy and Materials (HEREM), 2021
Edited by Mohan Lal Kolhe

Available online at:
stet-review.org

REGULAR ARTICLE OPEN ACCESS

Preparation and property analysis of solid carbonate-oxide composite materials for an electrolyte used in low-temperature solid oxide fuel cell

Yong-Xin Liang, Ze-Rong Ma, Si-Ting Yu, Xin-Yue He, Xu-Yang Ke, Ri-Feng Yan, Xiao-Xian Liang, Xin Wu, Rui-Sen Huang, Liang-Cheng Wen*, and Gengyu Cao*

College of Materials Science and Engineering, Guangdong University of Petrochemical Technology, 139 Guanduer Road, Maonan District, Maoming City 525000, Guangdong Province, PR China

Received: 4 October 2021 / Accepted: 4 February 2022

Abstract. The oxide-carbonate composite electrolyte material with high ionic conductivity at low temperature has been thought that it can be used to develop LT-SOFC. However, the carbonate composite electrolyte is not easy to make it dense, especially mixing and packing oxide and carbonate to fabricate the composite electrolyte simply. In this article, rare-earth-doped CeO_2 (RDC) (R = La, Sm, Gd, and Gd + Y) series samples were prepared by wet ball-milling, then sintered into fully dense and porous oxide bulk at 1500–1600 °C and 1000 °C. Melted carbonate LNCO, composed of Li_2CO_3 and Na_2CO_3 at a molar ratio of 1:1, was combined with porous oxide bulk materials using a bath method at 500 °C for 10 h to prepare a dense carbonate-oxide composite electrolyte. The dense oxide-carbonate composite electrolyte always obtains by this fabrication process. Boiling water was used to remove carbonate from these composites. Lattice parameters were obtained through Rietveld refinement, and a calculation procedure for quantifying the composite density was proposed. The quantified composite density results were verified through scanning electron microscopy microstructure observations. The Ce valence in the RDC oxides and RDC-carbonate composite was analyzed by X-ray absorption near edge structure spectroscopy to observe the effects of heat treatment temperature and carbonate on the Ce^{4+}/Ce^{3+} mixed-valence state in doped CeO_2.

Keywords: Solid electrolyte, Carbonate, Full dense, Mixed-valence states.

1 Introduction

Solid Oxide Fuel Cell (SOFC) technology has great potential in the power generation field. The structures of its components are simple and because SOFC technology can be used in high temperatures (650–1000 °C), it does not require use of expensive platinum as a catalytic converter because cathode and anode materials can be used at relatively low costs instead. Furthermore, SOFC technology has a high efficiency, relatively low pollution emissions, such as NOx, SOx, and HC, and the produced CO_2 can be easily captured [1, 2]. Additionally, the materials that can be used as fuels in an SOFC are diverse, including natural gas, CO, H_2, methanol, coal gas, and even flammable exhaust gases.

To popularize the use of SOFCs, some components still require further improvement. For instance, $(Y_{0.08}Zr_{0.92})O_{1.96}$ (8 mol% yttria-stabilized zirconia, 8YSZ) is currently a commercially available electrolyte ceramic material that has a low conductivity of 0.1 S cm^{-1} under operational temperatures of 1000 °C [3–5]. The use of a SOFC under high temperatures has the following disadvantages: (1) The composition interface is prone to reacting. (2) There can be a reduction in thermal stability. (3) Interfacial bonding is affected by the coefficient of expansion and easily results in battery cracking caused by thermal stress. (4) To achieve stable usage, electrode and bipolar plate materials with relatively high costs are required, directly affecting the manufacturing costs of the SOFC [6–10]. Electrolyte materials currently in use only possess appropriate levels of conductivity in high temperature environments. Therefore, the development of an electrolyte material with a high ionic conductivity in low temperature environments (under 600 °C) is an essential research topic in SOFC development.

In operational environments with temperatures below 600–800 °C, Rare-earth Doped CeO_2 (RDC) electrolyte materials can achieve conductivity values similar to that of 8YSZ at 1000 °C. Therefore, RDC is viewed as the

* Corresponding authors: 2032466104@qq.com; gyucao@gdupt.edu.cn

Table 1. Chemicals used in this study.

Reagent	Label	Purity
La_2O_3	*Riedel-de Haën*	99.9%
Sm_2O_3	*Riedel-de Haën*	99.9%
Gd_2O_3	*Riedel-de Haën*	99.9%
Y_2O_3	*Riedel-de Haën*	99.9%
Li_2CO_3	*Riedel-de Haën*	99.5%
Na_2CO_3	*Showa*	99%
PMMA (Poly(methyl methacrylate))	*Aldrich Chemical*	MW ~ 996 000
$C_3H_5(OH)_3$	*Junsei Chemical*	99%
CH_3COCH_3	*Acros Organics*	99.8%
Corn oil	*Junsei Chemical*	99.9%

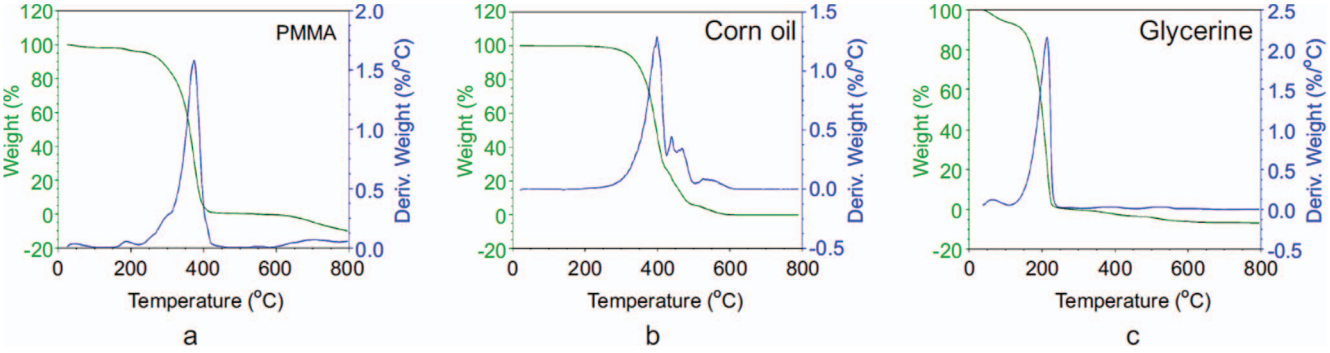

Fig. 1. TG/DTA diagrams of (a) binder (PMMA), (b) dispersant (corn oil), and (c) plasticizer (glycerin).

electrolyte material with the greatest potential for medium to low temperature applications. However, a portion of the Ce^{4+} may be reduced to Ce^{3+} in doped CeO_2 oxides during high-temperature sintering, which may result in a mixed-valence state. After the resulting material is used to assemble a cell component, if the operating temperature surpasses 550 °C and the material comes into contact with an anode reduction atmosphere, the formation of a Ce^{4+}/Ce^{3+} mixed-valence state is accelerated and the electrical conductivity is increased, which results in a decline in the open circuit voltage and operating power density [11–14].

In order to stop the Ce valence change, two electrolyte materials, a carbonate mixture and oxygen ion conductor, were combined to produce a carbonate-oxide composite; under 500 °C, it achieves a conductivity value similar to that of 8YSZ at 1000 °C and suppresses the Ce element valence change, which is an achievement that has attracted remarkable attention. This study builds upon previous research by synthesizing a carbonate-oxide composite electrolyte material through a bath method in order to ensure a high degree of density [15]. Furthermore, a series of doped CeO_2 oxides of $(La_{0.2}Ce_{0.8})O_{1.9}$ (LaDC), $(Sm_{0.2}Ce_{0.8})O_{1.9}$ (SDC), $(Gd_{0.2}Ce_{0.8})O_{1.9}$ (GDC), and $(Gd_{0.05}Y_{0.15}Ce_{0.8})O_{1.9}$ (GYDC) were synthesized for complete physical property analyses and discussion. The lattice parameter, microstructure and Ce^{4+}/Ce^{3+} mixed-valence state in the RDC oxides and carbonate-oxide composite materials are shown in this research.

2 Materials and methods

The chemicals listed in Table 1 were processed with wet ball-milling to produce the LaDC, SDC, GDC, and GYDC sample powders. The manufacturing process was as follows: 3 wt.% binder (PMMA), 1 wt.% dispersant (corn oil), and 1 wt.% plasticizer (glycerin) were added to each sample powder. The resultant mixture was placed in a tungsten carbide grinding jar. A suitable amount of zirconia balls with 1 cm diameters and a volume ratio of 1:1 relative to the sample powder were added. Acetone was added, and the resulting mixture was ground with a planetary ball mill for 24 h. After filtering out the zirconia balls and placing the solution into an oven to dry the acetone, an agate mortar was used to evenly grind the dry powder. A uniaxial pressure of 840 MPa was then applied to transform the powder sample into a pellet. The pellet was placed into a furnace that increased 100 °C/h until 500 °C, after which the furnace idled for 2 h to remove any remaining organic additives. The ThermoGravimetric and Differential Thermal Analysis (TG/DTA) results of the binder, dispersant, and plasticizer are shown in Figure 1. The heat program was used by the heating rate of 5 °C/min from room temperature to 800 °C, and the N_2 gas was employed to measurement process by 20 mL/min. These results indicate that these organic additives can be completely decomposed at 500 °C. Then, the furnace continued to increase its temperature by 100 °C/h until it reached the maximal sintering

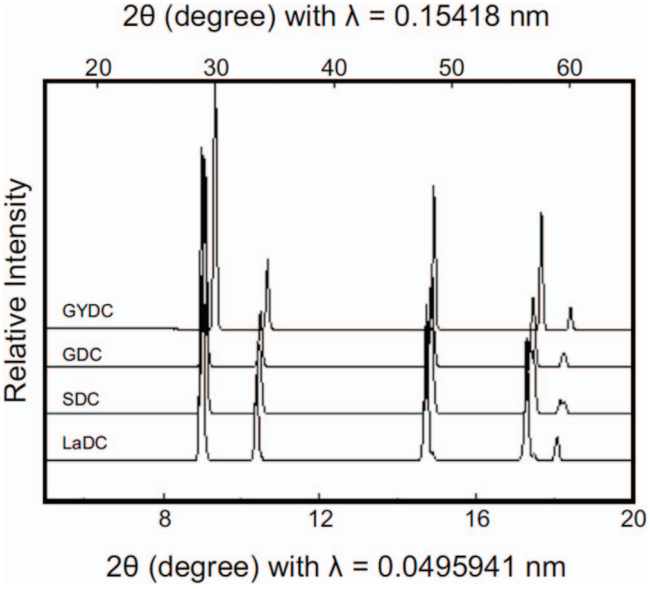

Fig. 2. XRD diagram of the RDC series oxides sintered at 1500–1600 °C for 5 h. The angle of diffraction 2θ values are for *X*-wavelength 0.15418 nm (top) and 0.0495941 nm (bottom).

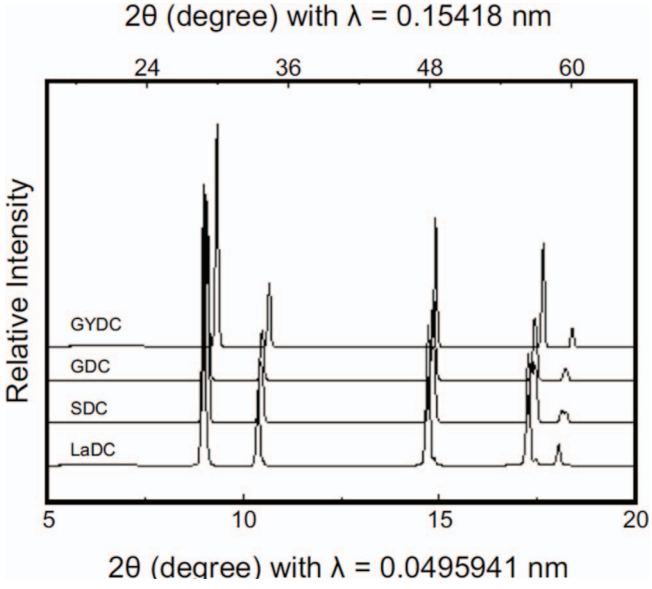

Fig. 3. XRD diagram of the RDC series oxides sintered at 1000 °C for 10 h. The angle of diffraction 2θ values are for *X*-wavelength 0.15418 nm (top) and 0.0495941 nm (bottom).

temperature of 1500–1600 °C, at which point, the furnace maintained the temperature to complete sintering over 5–10 h. Finally, the furnace lowered its temperature by 100 °C/h until it reached 1000 °C, at which point, the furnace was turned off to allow for natural cooling.

The theoretical density of each sample was calculated by first obtaining the theoretical molar volume: $a^3 \times 10^{-24} \times 6.02 \times 10^{23}\ \mathrm{cm}^3/Z$, in which a (Å) is the sample unit cell parameter. If the sample exhibited a fluorite structure, Z equals 1, whereas if the sample exhibited a pyrochlore structure, which is the superstructure of fluorite, Z equals 8. This is because the entire cells were $A_{16}B_{16}O_{56}$ and the typical $A_2B_2O_7$ is 1/8 of the unit cell. Then, the molar weight of the sample was divided by the theoretical molar volume to obtain the theoretical density of each sample. Next, a scale was used to measure the actual weight of each sample, after which the Archimedes principle was used to determine the actual volume, from which the actual density was obtained. Lastly, the actual density was divided by the theoretical density to find the relative density of the sample.

The manufacturing process of composites was as follows. First, the RDC pellet was sintered at the appropriate temperature into a porous oxide bulk material that has a relative density of approximately 60–70%. Then, Li_2CO_3 and Na_2CO_3 were mixed through wet-ball milling at a 1:1 molar ratio to produce a carbonate mixture referred to as LNCO. An appropriate amount of LNCO was then placed into an SUS304 stainless steel container that was heat resistant up to 900 °C. The container was heated to 500 °C for 24 h to produce a carbonate liquid. A porous oxide pellet was then heated with the LNCO to 500 °C for 12 h to allow the melted carbonate to penetrate and fill the pores of the pellet in order to produce a high-density composite. Zhu *et al.* found that the conductivity

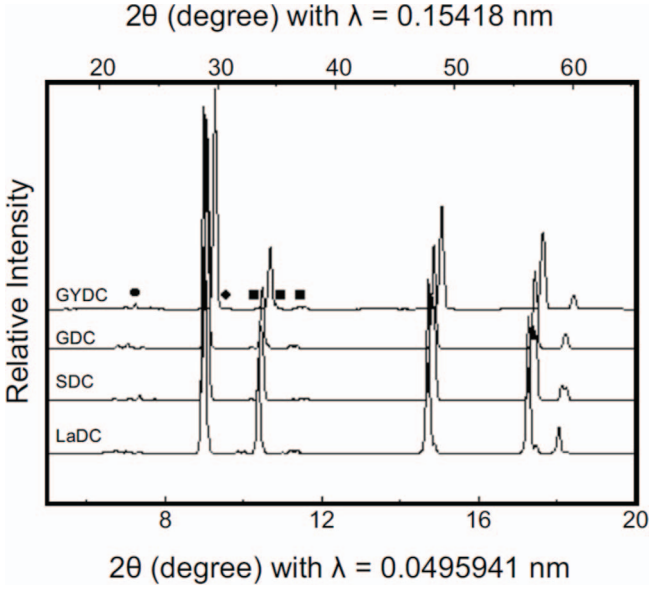

Fig. 4. XRD diagram of the RDC series composites. The angle of diffraction 2θ values are for *X*-wavelength 0.15418 nm (top) and 0.0495941 nm (bottom). The symbol (●) in the diagram indicates the Li_2CO_3 signal, whereas (■) indicates the Na_2CO_3 signal.

of the carbonate-oxide composite increases with increasing the amount of carbonate mixture until the carbonate volume makes up 30% of the composite [16]. Therefore, this study utilized sintering temperatures to make oxide bulk materials with porosity values between 30% and 40%, which is equal to the ratio of carbonate volumes in the samples.

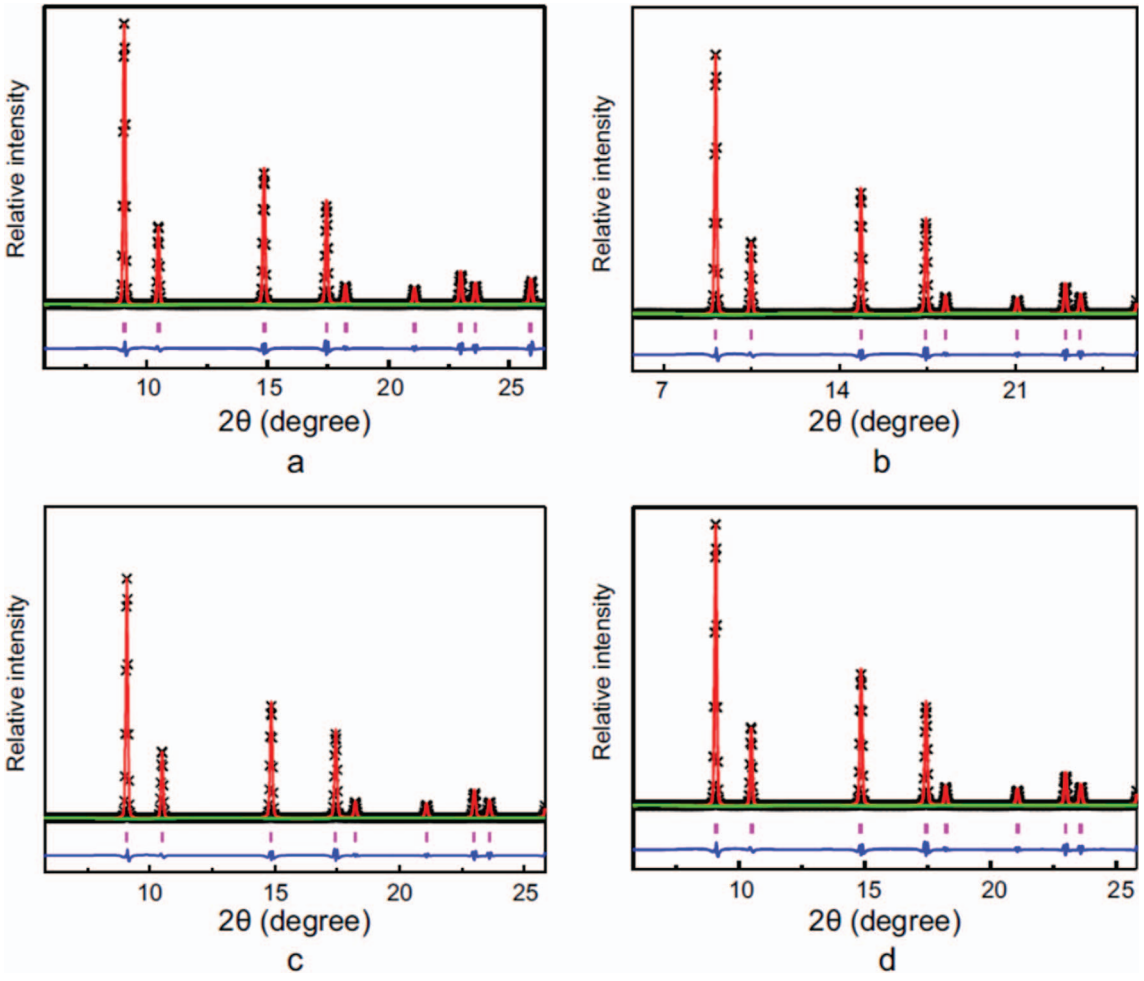

Fig. 5. The RDC series Rietveld refinement results for sample powders sintered at 1500–1600 °C, (a) LaDC, (b) SDC, (c) GDC, and (d) GYDC.

Powder diffraction data used for the Rietveld refinement were collected to determine the crystal structure of the sample oxide. The General Structure Analysis System developed by Larson and von Dreele was employed to analyze the structural parameters using the Rietveld method [17]. The morphology of the sample was observed using a VEGA SBH scanning electron microscope. The X-ray Absorption Near Edge Structure spectroscopy (XANES), BL16A1 wiggler beam line was used to observe the Ce^{4+}/Ce^{3+} mixed-valence state in both the RDC oxides and carbonate-oxide composite materials.

3 Results and discussion

Figure 2 illustrates the XRD diagram for LaDC, SDC, GDC, and GYDC pure oxide samples. Here, GDC and GYDC were sintered at 1500 °C for 5 h, while LaDC and SDC were sintered at 1600 °C for 5 h. These temperatures were selected so that the pure oxide sample bulks would exceed the relative density of 98.3(4)%, which meant that the density would be as high as an SOFC solid electrolyte. The sintered RDC series samples were all fluorite single-phase samples. As can be observed from Figures 2 and 3, the diffraction signal angles gradually shift toward the right from LaDC, SDC, GDC, to GYDC because of the respective eight coordination La^{3+}, Sm^{3+}, Gd^{3+} and Y^{3+} ionic radii of 1.16, 1.079, 1.053, and 1.019 Å [18]. This trend matches the Bragg diffraction formula of $n\lambda = 2d\sin\theta$. Figure 3 shows the XRD diagram for the LaDC, SDC, GDC, and GYDC pure oxide samples sintered at 1000 °C for 10 h. These samples also exhibited fluorite single-phase structures. Figure 4 displays the XRD diagram of the carbonate-oxide composites and LNCO. It shows the signal positions of the Li_2CO_3 (7.12° and 10.64°) and Na_2CO_3 (8.90°, 11.13°, 11.47°, and 14.09°) [15]. As the carbonate structures were amorphous, their signal range was wider and less apparent [6].

The XRD angle of diffraction data from the RDC samples was refined to obtain the structural parameters for calculating the relative density of the samples and to evaluate their effect on sample physical properties. Figure 5

Table 2. LaDC, SDC, GDC, and GYDC lattice parameters, χ^2, R_{wp}, and R_p values.

Sample	*a*-axis	χ^2	R_{wp} (%)	R_p (%)
LaDC	5.4726(7)	3.975	3.55	2.24
SDC	5.4370(2)	3.115	3.91	3.23
GDC	5.4237(6)	3.415	2.32	1.62
GYDC	5.4106(4)	4.006	2.58	1.33

shows the Rietveld refinement results for the RDC series samples sintered at 1500–1600 °C. Table 2 lists the RDC series sample lattice parameters obtained from the Rietveld refinement. Note that the χ^2 values are all between 0.5 and 5 and the error values are less than 5%, indicating that the sample calculations are credible. Figure 6 shows the refined lattice parameters plotted against the doped rare earth ionic radii. The sample lattice parameters, including LaDC, SDC, GDC, and GYDC, exhibit a gradually decreasing trend that is consistent with Vegard's Law. These results indicate that, for this series, the consistency of each step in the manufacturing process of the samples is high and human error is relatively small.

The heat treatment temperatures and relative densities of the RDC series of high-density oxides, porous oxides, and composite samples are listed in Table 3. As shown in the table, both LaDC and SDC sintered at 1600 °C, and GDC and GYDC sintered at 1500 °C produced high sample densities (>98.3(4)%). Furthermore, 1000 °C sintering for 10 h produced densities between 63.6(2)% and 68.4(5)%, which correspond to porosities between 31.6% and 36.4%. After the porous samples were made into composites, the sample densities approached 100%, meaning that the melted carbonate filled almost all the sample pores. A necessary condition for a solid electrolyte is high relative density close to 100%. This study verified the relative density of composites, as shown in Table 4. The composite made of a porous oxide with a known relative density, then used sandpaper to remove the excess surface carbonate of the composite bulk and measured it to determine weight W_1. Then, boiling water was used to remove the carbonate in the composite, which was then dried prior to reweighing to obtain the weight W_2 of the remaining oxide bulk. Therefore, $W_1 - W_2$ was the weight of the carbonate filling into the porous oxide bulk. As LNCO is composed of Li_2CO_3 and Na_2CO_3 with a molar ratio of 1:1, the respective weights, W_3 and W_4, in the composite can be obtained. The densities of Li_2CO_3 and Na_2CO_3 were used to obtain their respective volumes V_4 and V_5 in the composite filling. The volumes of Li_2CO_3 and Na_2CO_3 ($V_4 + V_5$) approached volume V_3 of the oxide bulk material pores, indicating that the carbonate almost completely filled the pores. Furthermore, the relative density of the oxide can be used to obtain the volume of the oxide V_2 in the composite. The sum of the two carbonate volumes $V_4 + V_5$ plus the volume occupied by the oxide V_2, divided by the volume of the composite V_1 is a value closely approaching 1. These results confirm that this calculation process and its results can be used to quantify the relative density of a carbonate-oxide composite bulk.

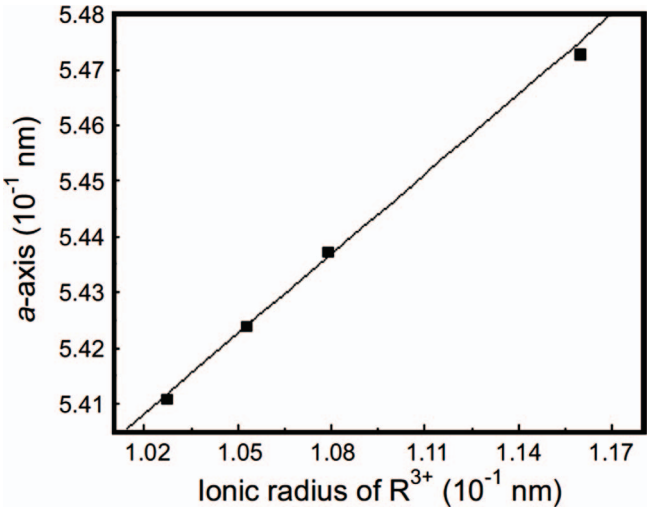

Fig. 6. LaDC, SDC, GDC, and GYDC lattice parameters plotted against R^{3+} ionic radius.

Table 3. RDC and RDC composite heat treatment temperatures and relative densities.

Sample	Relative density (%)		
	1500–1600 °C	1000 °C	Composite
LaDC	98.3(4)	66.5(6)	99.8(2)
SDC	98.9(5)	63.6(2)	100.0(3)
GDC	99.4(2)	68.4(5)	99.7(1)
GYDC	98.5(6)	64.8(4)	99.4(2)

Scanning Electron Microscope (SEM) microstructure photographs help visualize the results of the high-density composite calculations. Figure 7 shows the SEM images of the RDC series high-density oxide, porous oxide, and composite samples magnified 5000 times. As shown in Figures 7a–7d, pores are barely visible in oxides that have been sintered at high temperatures (1500–1600 °C), whereas numerous pores can be seen in the oxide samples sintered at 1000 °C in Figures 7e–7h. Figures 7i–7l depict the SEM diagrams of the composite samples and clearly illustrate that the vast majority of pores in the porous oxide samples have been filled.

Numerous studies have indicated that after CeO_2-doped oxide electrolyte materials are assembled into SOFC unit cell components, the reduction of Ce^{4+} into Ce^{3+} results in a mixed-valence state. This study proposes that materials of this type are likely to begin producing mixed-valence states during high-temperature sintering densification process. Operational temperatures higher than 550 °C and the effects of the reductive environment result in an even more apparent mixed-valence phenomenon. The resulting electronic conductivity is increased, causing lower open

Table 4. Carbonate composite density calculation process and results.

Sample	Composite W_1 (g)	Oxide W_2 (g)	Carbonate $W_1 - W_2$ (g)	Li_2CO_3 W_3 (g)	Na_2CO_3 W_4 (g)
LaDC	1.4101	1.2041	0.2060	0.0846	0.1214
SDC	1.4133	1.2131	0.2002	0.0822	0.1180
GDC	1.4281	1.2352	0.1929	0.0792	0.1136
GYDC	1.4064	1.1900	0.2164	0.0889	0.1275

Sample	Oxide relative density (%)	Composite V_1 (cm^3)	Oxide V_2 (cm^3)	Void V_3 (cm^3)
LaDC	66.7	0.2653	0.1770	0.0884
SDC	67.4	0.2641	0.1780	0.0861
GDC	68.4	0.2616	0.1789	0.0827
GYDC	64.8	0.2632	0.1706	0.0926

Sample	Li_2CO_3 V_4 (cm^3)	Na_2CO_3 V_5 (cm^3)	Carbonate $V_4 + V_5$ (cm^3)	Composite density $(V_4 + V_5 + V_2)/V_1$ (%)
LaDC	0.0401	0.0480	0.0881	99.7
SDC	0.0390	0.0466	0.0856	99.4
GDC	0.0375	0.0449	0.0825	99.8
GYDC	0.0421	0.0504	0.0925	99.9

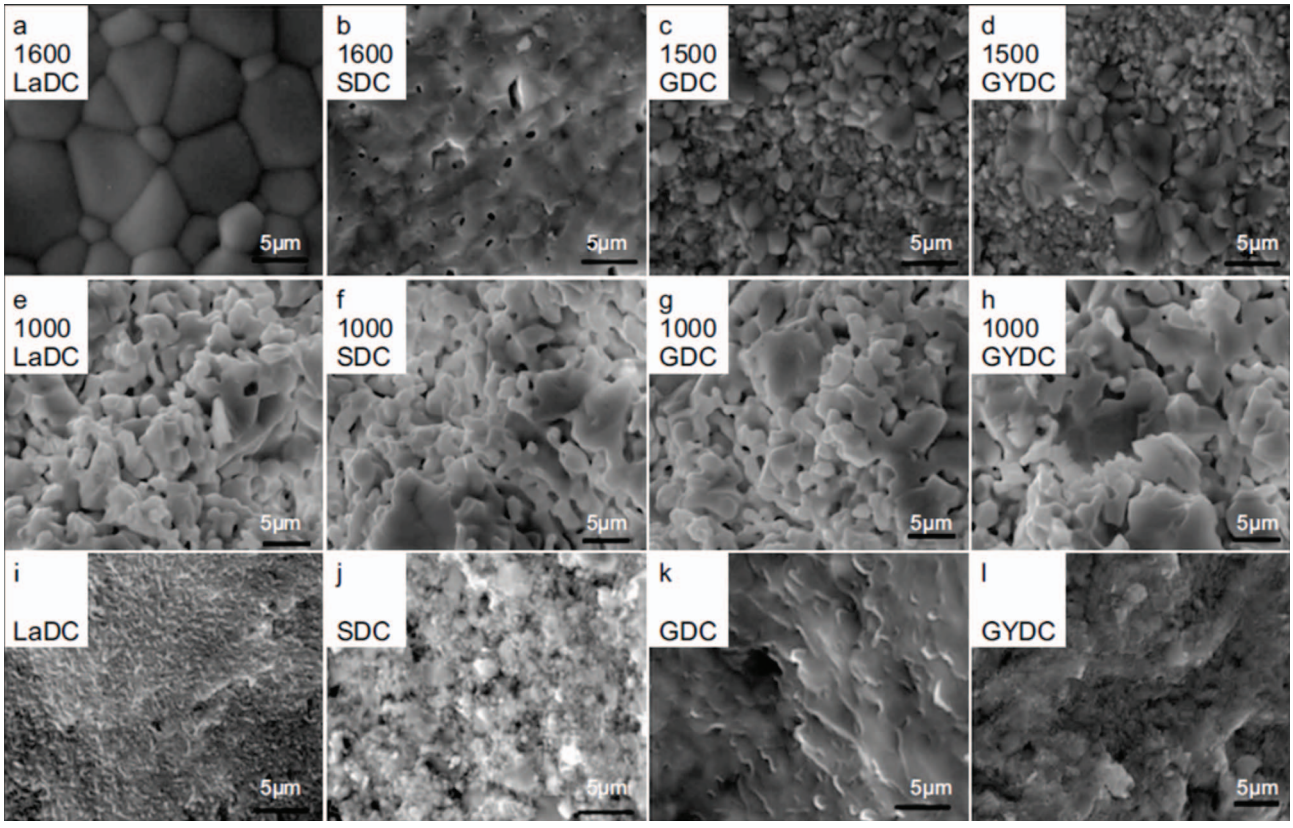

Fig. 7. RDC sintered at 1500–1600 °C for 5 h; sintered at 1000 °C for 10 h; SEM diagram of carbonate composite magnified 5000 times. (Here, (a), (e), (i) have R = La; (b), (f), (j) have R = Sm; (c), (g), (k) have R = Gd; (d), (h), (l) have R = Gd + Y.)

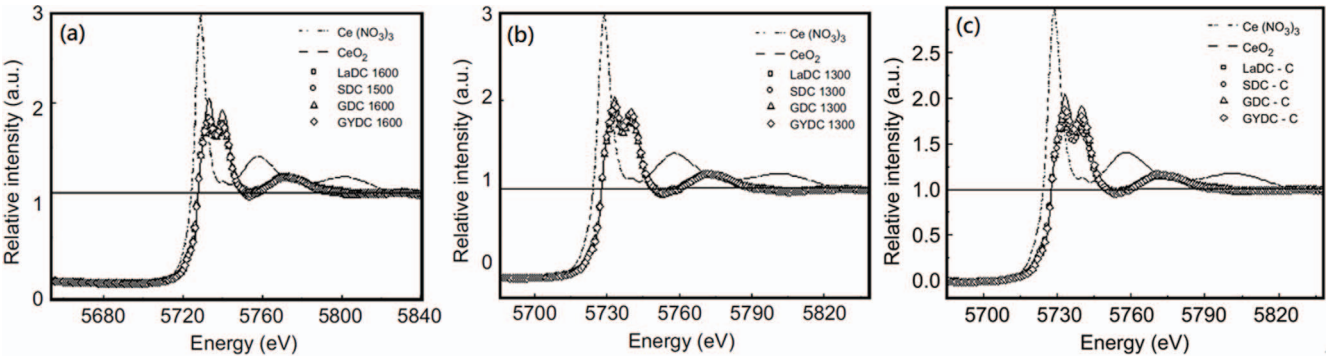

Fig. 8. (- – -) $Ce(NO_3)_3$, (–) CeO_2, (□) LaDC, (○) SDC, (Δ) GDC, and (◇) GYDC samples with 1500–1600 °C (a), 1000 °C (b), and composite samples with 500 °C (c) treatment, Ce *L*-edge XANES spectrum after normalization.

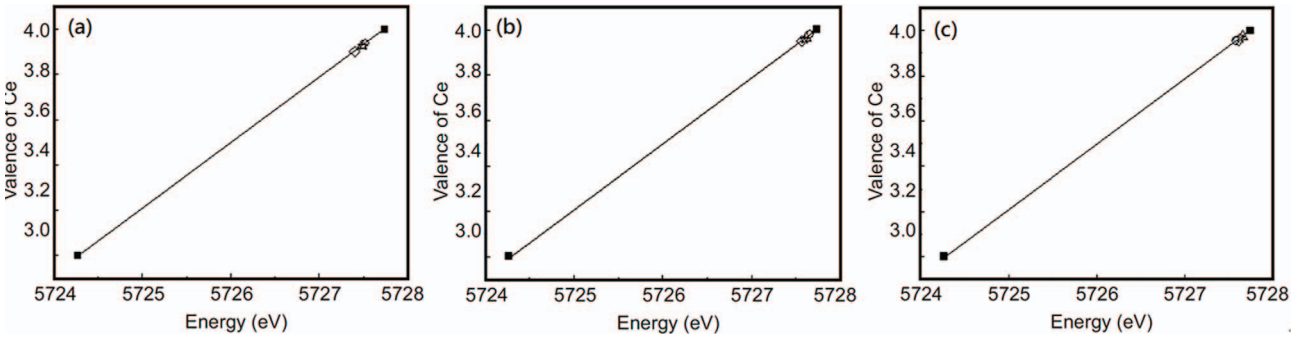

Fig. 9. $Ce(NO_3)_3$ and CeO_2 reference standard, (□) LaDC, (○) SDC, (Δ) GDC, and (◇) GYDC samples treated with 1500–1600 °C (a), 1000 °C (b), and composite samples with 500 °C (c); valence plot of maximal first order differential values of Ce element.

circuit values, which adversely affect the operation power density of the SOFC single cell. Therefore, this study utilized typical high-temperature sintering densification on the RDC oxides, low-temperature heat-treated samples, and sample powders resulting from composite production, with $Ce(NO_3)^3$ and CeO_2 as reference standards to analyze the average Ce valence.

The RDC series oxide measured by XANES spectrum approached that of the CeO_2 reference standard, exhibiting single maximum differential energy shoulders that were almost identical. Thus, this study used the strength "1" position as the RDC series reference line, as shown by the horizontal lines in Figure 8. Each energy shoulder at the intersection between each energy reference line and spectrum was used to infer the Ce element valence of each sample, as shown in Figure 9. The analysis results indicated that the RDC samples that underwent high temperature treatments exhibited lower Ce valences with an average of 3.93(2), whereas the RDC samples treated at 1000 °C temperatures exhibited higher Ce valences with an average of 3.96(1). Thus, a multi-valence element, like Ce, might tend to reduce its state during higher heat-treated temperatures. The RDC oxides were first sintered at 1000 °C to get a porous sample bulk, followed by 500 °C treatments with the LNCO carbonate mixture. The resultant average valence of Ce in the composite was 3.96(1), which is similar to the RDC oxides treated at 1000 °C. The Ce valence in the RDC oxides with different heat-treated temperature and in the carbonate-oxide composites measured by XANES are listed in Tables 5–7. As seen in the results, the Ce valence in the RDC oxide would not be affected by combining with carbonate. In other words, using the LNCO carbonate and RDC oxide to form a composite creates a stable electrolyte material that can be applied in low temperature SOFCs.

Table 5. $Ce(NO_3)_3$, CeO_2 and LaDC, SDC, GDC, and GYDC sample powders with 1500–1600 °C treatment: Ce *L*-edge XANES spectrum single maximum differential energy shoulders and corresponding Ce valence.

x	Energy (eV)	Valence
$Ce(NO_3)_3$	5724.3	3
CeO_2	5727.7	4
LaDC-1600	5727.5	3.94
SDC-1600	5727.5	3.94
GDC-1500	5727.4	3.90
GYDC-1500	5727.5	3.94
Average		3.93(2)

Table 6. $Ce(NO_3)_3$, CeO_2 and LaDC, SDC, GDC, and GYDC sample powders with 1000 °C treatment: Ce *L*-edge XANES spectrum single maximum differential energy shoulders and corresponding Ce valence.

x	Energy (eV)	Valence
$Ce(NO_3)_3$	5724.3	3
CeO_2	5727.7	4
LaDC	5727.7	3.97
SDC	5727.6	3.96
GDC	5727.6	3.96
GYDC	5727.7	3.97
Average		3.96(1)

Table 7. $Ce(NO_3)_3$, CeO_2 and LaDC, SDC, GDC, and GYDC composite sample powders with 500 °C treatment: Ce *L*-edge XANES spectrum single maximum differential energy shoulders and corresponding Ce valence.

x	Energy (eV)	Valence
$Ce(NO_3)_3$	5724.3	3
CeO_2	5727.7	4
LaDC–C	5727.6	3.96
SDC–C	5727.7	3.97
GDC–C	5727.6	3.96
GYDC–C	5727.7	3.97
Average		3.96(1)

4 Conclusion

The XRD structure appraisal and Rietveld refinement results indicated that the RDC oxide samples produced through the solid-state synthesis method possess a single-phase fluorite phase. When the samples were assembled into bulk materials, sintering them at 1500–1600 °C achieved relative densities exceeding 98.3%, whereas sintering at 1000 °C for 10 h maintained densities between 63.6(2)% and 68.4(5)%, indicating porosities between 31.6% and 36.4%. The bath method was used to heat porous oxide bulk materials with a carbonate mixture, LNCO, to 500 °C for 12 h, then allowing the melted carbonate to fill the oxide pores and produce a dense carbonate-oxide composite electrolyte. Boiling water was used to remove the carbonate. Then, structural refinement was used to obtain the lattice parameters for the pore and oxide volume calculations. The volume of LNCO used to fill the pores approached the volume of the pores of the RDC oxide sintered at 1000 °C, indicating that the melted carbonate permeated and filled the oxide pores. This result was supported by the SEM observations. The XANES spectrum analysis results indicated that the RDC samples sintered at 1500–1600 °C exhibited a lower average Ce valence of 3.93(2), while samples treated at 1000 °C exhibited a higher average Ce valence of 3.96(1), which is identical to that of the composite samples. These results illustrate that a carbonate-oxide composite is a stable electrolyte material for manufacturing under lower temperatures to further inhibit the development of Ce^{4+}/Ce^{3+} mixed-valence situations. The composite electrolyte has potential for low temperature SOFC operation under 500 °C. This can increase the working performance and decrease the degradation rate of the peripheral components. Thus, the fabrication cost can be further decreased to improve market acceptance.

Conflicts of interest

The authors declare that they have no conflict of interest.

Data availability

The datasets used and/or analysed during the current study are available from the corresponding author on reasonable request.

Authors' contributions

Conceptualization, Yong-Xin Liang, Xin Wu, L.C. Wen, and Gengyu Cao; methodology, Yong-Xin Liang, L.C. Wen, and Ze-Rong Ma; software, Yong-Xin Liang, Rui-Sen Huang, and Si-Ting Yu; validation, Xin-Yue He, L.C. Wen, and H.M. Liu; formal analysis, Yong-Xin Liang, L.C. Wen, and Xu-Yang Ke; investigation, Yong-Xin Liang, Ze-Rong Ma, L.C. Wen, and Ri-Feng Yan; resources, Yong-Xin Liang, L.C. Wen, and Xiao-Xian Liang; data curation, L.C. Wen and Gengyu Cao; writing – original draft preparation, Yong-Xin Liang, L.C. Wen; writing – review and editing, Yong-Xin Liang, Ze-Rong Ma, L.C. Wen, and Gengyu Cao; visualization, Yong-Xin Liang, L.C. Wen; supervision, L.C. Wen; project administration, L.C. Wen and Gengyu Cao; funding acquisition, Gengyu Cao. All authors have read and agreed to the published version of the manuscript.

Acknowledgments. This research was funded by the *Development and Testing of ITSOFC Single Cell*, which belongs to the *Skilled Personnel Recommend Programme of Guangdong University of Petrochemical Technology*, grant number 702-519150.

Funding

This research was funded by the Development and Testing of ITSOFC Single Cell, which belongs to the Skilled Personnel Recommend Programme of Guangdong University of Petrochemical Technology, grant number 702-519150.

References

1 Lara C., Pascual M.J., Durán A. (2007) Chemical compatibility of RO–BaO–SiO_2 (R = Mg, Zn) glass-ceramic seals with SOFC components, *J. Glass Sci. Technol. B* **48**, 218–224.

2 Lashtabeg A, Skinner S.J. (2006) Solid oxide fuel cells – a challenge for materials chemists, *J. Mater. Chem.* **16**, 3161–3170.

3 Gao H., Liu J., Chen H., Li S., He T., Ji Y., Zhang J. (2008) The effect of Fe doping on the properties of SOFC electrolyte YSZ, *Solid State Ion.* **179**, 1620–1624.

4 Singhal S.C., Kendall K. (2003) *High temperature solid oxide fuel cells: Fundamentals, design and applications*, 1st edn., Elsevier, Oxford, UK.

5 West A.R. (1999) *Basic solid state chemistry*, Wiley, New York, USA.

6 Tang Z., Lin Q., Mellander B.E., Zhu B. (2010) SDC–LiNa carbonate composite and nanocomposite electrolytes, *In. J. Hydrogen Energy* **35**, 2970–2975.

7 Zhu B., Yang X.T., Xu J., Zhu Z.G., Ji S.J., Sun M.T., Sun J.C. (2003) Innovative low temperature SOFCs and advanced materials, *J. Power Sources* **118**, 47–53.

8 Mat M.D., Liu X., Zhu Z., Zhu B. (2007) Development of cathodes for methanol and ethanol fuelled low temperature (300–600 °C) solid oxide fuel cells, *Int. J. Hydrogen Energy* **32**, 796–801.

9 Zhu B., Liu X., Schober T. (2004) Novel hybrid conductors based on doped ceria and BCY20 for ITSOFC applications, *Electrochem. Commun.* **6**, 378–383.

10 Pikalova E.Y., Maragou V.I., Demina A.N., Demin A.K., Tsiakaras P.E. (2008) The effect of co-dopant addition on the properties of $Ln_{0.2}Ce_{0.8}O_2 - \delta$ (Ln = Gd, Sm, La) solid-state electrolyte, *J. Power Sources* **181**, 199–206.

11 Steele B.C. (1994) Oxygen transport and exchange in oxide ceramics, *J Power Sources* **49**, 1–4.

12 Steele B.C. (1995) Interfacial reactions associated with ceramic ion transport membranes, *Solid State Ion.* **75**, 157–165.

13 Steele B.C. (2000) Appraisal of $Ce_{1-y}Gd_yO_{2-y/2}$ electrolytes for IT-SOFC operation at 500 °C, *Solid State Ion.* **129**, 95–110.

14 Xia C., Chen F., Liu M. (2001) Reduced-temperature solid oxide fuel cells fabricated by screen printing, *Electrochem. Solid-State Lett. A* **4**, 52–54.

15 Wen L.C., Hsieh C.Y., Tsai Y.I., Lin H.K., Chang S.C., Kao H.C., Sheu H.S., Lee M.C., Lee Y.S. (2013) Electrical properties of Sm-doped Ceria (SDC) and SDC carbonate composite, *J. Chin. Chem. Soc.* **60**, 1359–1364.

16 Zhu W., Xia C., Ding D., Shi X., Meng G. (2006) Electrical properties of ceria-carbonate composite electrolytes, *Mater. Res. Bull.* **41**, 2057–2064.

17 Larson A.C., von Dreele R.B. (2003) *General structure analysis system*. Report La-UR-86-748. Los Alamos National Laboratory, Los Alamos.

18 Shannon R.T. (1974) Revised effective ionic radii and systematic studies of interatomic distances in halides and chalcogenides, *Acta Crystallogr. A* **32**, 751–767.